The Astrophysical Journal, 808:73 (15pp), 2015 July 20 doi:10.1088/0004-637X/808/1/73

THE OPTICALLY UNBIASED GRB HOST (TOUGH) SURVEY. VII. THE HOST GALAXY LUMINOSITY FUNCTION: PROBING THE RELATIONSHIP BETWEEN GRBs AND STAR FORMATION TO REDSHIFT ~6

S. Schulze[1,2,3], R. Chapman[3,4], J. Hjorth[5], A. J. Levan[6], P. Jakobsson[3], G. Björnsson[3], D. A. Perley[7,14], T. Krühler[8], J. Gorosabel[9,10,11], N. R. Tanvir[12], A. de Ugarte Postigo[5,9], J. P. U. Fynbo[5], B. Milvang-Jensen[5], P. Møller[13], and D. J. Watson[5]

[1] Instituto de Astrofísica, Facultad de Física, Pontificia Universidad Católica de Chile, Vicuña Mackenna 4860, 7820436 Macul, Santiago, Chile; sschulze@astro.puc.cl
[2] Millennium Institute of Astrophysics, Vicuña Mackenna 4860, 7820436 Macul, Santiago, Chile
[3] Centre for Astrophysics and Cosmology, Science Institute, University of Iceland, Dunhagi 5, 107 Reykjavík, Iceland
[4] Centre for Astrophysics Research, University of Hertfordshire, Hatfield, Herts AL10 9AB, UK
[5] Dark Cosmology Centre, Niels Bohr Institute, University of Copenhagen, Juliane Maries Vej 30, DK-2100 Copenhagen Ø, Denmark
[6] Department of Physics, University of Warwick, Coventry, CV4 7AL, UK
[7] Department of Astronomy, California Institute of Technology, MC 249-17, 1200 East California Blvd., Pasadena CA 91125, USA
[8] European Southern Observatory, Alonso de Córdova 3107, Vitacura Casilla 19001, Santiago, Chile
[9] Instituto de Astrofsica de Andalucía, Consejo Superior de Investigaciones Científicas (IAA-CSIC), Glorieta de la Astronomía s/n, E-18008 Granada, Spain
[10] Unidad Asociada Grupo Ciencias Planetarias UPV/EHU-IAA/CSIC, Departamento de Física Aplicada I, E.T.S. Ingeniería, Universidad del País Vasco UPV/EHU, Alameda de Urquijo s/n, E-48013 Bilbao, Spain
[11] Ikerbasque, Basque Foundation for Science, Alameda de Urquijo 36-5, E-48008 Bilbao, Spain
[12] Department of Physics and Astronomy, University of Leicester, University Road, Leicester LE1 7RH, UK
[13] European Southern Observatory, Karl-Schwarzschildstrasse 2, D-85748, Garching, Germany
Received 2015 March 13; accepted 2015 June 3; published 2015 July 17

ABSTRACT

Gamma-ray bursts (GRBs) offer a route to characterizing star-forming galaxies and quantifying high-z star formation that is distinct from the approach of traditional galaxy surveys: GRB selection is independent of dust and probes even the faintest galaxies which can evade detection in flux-limited surveys. However, the exact relation between the GRB rate and the star formation rate (SFR) throughout all redshifts is controversial. The Optically Unbiased GRB Host (TOUGH) survey includes observations of all GRB hosts (69) in an optically unbiased sample of *Swift* GRBs; we utilize these to constrain the evolution of the UV GRB-host-galaxy luminosity function (LF) between $z = 0$ and $z = 4.5$, and compare this with LFs derived from both Lyman-break galaxy (LBG) surveys and simulation modeling. At all redshifts we find the GRB hosts to be most consistent with an LF derived from SFR weighted models incorporating GRB production via both metallicity-dependent and independent channels with a relatively high level of bias toward low metallicity hosts. In the range $1 < z < 3$ an SFR weighted LBG derived (i.e., non-metallicity biased) LF is also a reasonable fit to the data. Between $z \sim 3$ and $z \sim 6$, we observe an apparent lack of UV bright hosts in comparison with LBGs, though the significance of this shortfall is limited by nine hosts of unknown redshift.

Key words: galaxies: evolution – galaxies: luminosity function, mass function – galaxies: star formation – gamma-ray burst: general

1. INTRODUCTION

The past decade in extragalactic astronomy has been characterized by a tremendous increase in the understanding of the properties of high-z galaxies (for reviews see, e.g., Wolfe et al. 2005; Shapley 2011; Carilli & Walter 2013), such as the diversity and evolution of their star formation rate (SFR) histories (Pettini et al. 2002; Hopkins 2004; Hopkins & Beacom 2006; Bouwens et al. 2007, 2010a), the relation between stellar mass and luminosity (Pettini et al. 2001; Magdis et al. 2010; Schaerer et al. 2013), the relation between mass and metallicity (e.g., Tremonti et al. 2004; Savaglio et al. 2005; Erb et al. 2006; Lee et al. 2006; Foster et al. 2012) and the nature of extinction as a function of luminosity (Meurer et al. 1999; Calzetti et al. 2000). This progress has been driven by multi-band flux-limited surveys of ever-improving depth and coverage permitting the study of galaxies at redshifts ranging from $z = 0$–10 (e.g., Scoville et al. 2007; Bouwens et al. 2014).

These surveys are, however, not suited to assessing the contribution of the faintest galaxies to the cosmic star formation history. Gamma-ray burst (GRB) selected galaxy studies provide a complementary approach to constrain galaxy evolution across the whole mass spectrum (Perley et al. 2009; Krühler et al. 2011; Rossi et al. 2012) and from very low to very high redshift (the most distant GRB with a spectroscopic redshift known to date is GRB 090423 at $z = 8.2$, Tanvir et al. 2009; Salvaterra et al. 2009). The advantage of GRB-selected galaxy studies is that GRB production requires (in its simplest form) only a massive star (for a review see Woosley 2011 and references therein), which makes their detection independent of galaxy luminosity.

The exact relation between the GRB rate and the SFR is controversial: while long-duration GRBs are produced by massive stars and sample the entire range of known star-forming galaxies from faint dwarfs up to luminous Lyman-break galaxies (LBGs; Steidel et al. 1996) and sub-millimeter galaxies (e.g., Christensen et al. 2004; Tanvir et al. 2004; Fruchter et al. 2006; Michałowski et al. 2008; Savaglio et al. 2009; Krühler et al. 2011; Rossi et al. 2012; Perley

[14] Hubble Fellow.

et al. 2013; Hunt et al. 2014; Schady et al. 2014; Kohn et al. 2015), most of our knowledge is based on heterogeneous samples. Several GRB luminosity function (LF) and redshift distribution studies (e.g., Kistler et al. 2008; Jakobsson et al. 2012; Robertson & Ellis 2012) have found that the numbers of GRBs produced at high redshift imply that either the global SFR density is greater at high redshift than that found from LBG surveys, or that GRB production efficiency increases with redshift. Other authors consider that this result can be explained by continuing observational and redshift biases in existing GRB surveys (e.g., Elliott et al. 2012). In this work, we approach this question from the unique standpoint of having observations of the properties of the individual hosts of each burst in an observationally unbiased GRB sample, thus providing a complementary approach to simulation studies.

"The Optically Unbiased GRB Host" (TOUGH) survey by Hjorth et al. (2012) is the first such survey to make use of the strategic advantage of *Swift* to realize the production of a GRB host galaxy sample selected solely by accurate X-ray localization and VLT observability and unbiased by optical criteria such as afterglow detection or brightness. In this paper, we compare the evolution of the UV LF of GRB host galaxies to both those derived from LBG samples and those predicted from stellar population synthesis models (Trenti et al. 2014) which include both metallicity dependent and independent channels for GRB production.

Throughout the paper, we assume a ΛCDM cosmology with $H_0 = 71$ km s^{-1} Mpc^{-1}, $\Omega_m = 0.27$, and $\Omega_\Lambda = 0.73$ (Larson et al. 2011). All reported magnitudes are given in the AB system, and uncertainties are given at a 1σ confidence level, if not stated otherwise.

2. OBSERVATIONS AND DATA REDUCTION

2.1. The TOUGH Survey

The TOUGH survey targeted 69 GRBs in the R and K_s bands with FORS2 and ISAAC reaching limiting magnitudes of R (AB) $\sim$ 27.3 mag and K_s(AB) $\sim$ 23.4 mag at a 3σ confidence level. About 80% have a detected host galaxy (Hjorth et al. 2012; see also D. Malesani et al. 2015, in preparation) and thanks to ongoing spectroscopic follow-up observations >87% now have a measured redshift (Jakobsson et al. 2012; Krühler et al. 2012, 2015). In addition, the hosts between $z = 2$ and $z = 4.5$ were targets of a moderately deep spectroscopy campaign to study Lyα in emission, and hosts at $z < 1$ were part of a radio survey. These campaigns allowed the investigation of several properties such as the $(R - K_s)$ color and the offset distribution (Hjorth et al. 2012; D. Malesani et al. 2015, in preparation), the redshift distribution (P. Jakobsson et al. 2012), the Lyα recovery rate (Milvang-Jensen et al. 2012), and the unobscured SFR inferred from radio observations for the hosts at $z < 1$ (Michałowsk et al. 2012).

2.2. New Data and Their Reduction

The VLT R-band data build the foundation of this paper. We complement this data set with *HST* observations via a dedicated GRB host program (PI: A. J. Levan), which targeted nearly all $3 < z < 4$ hosts. At $z \lesssim 0.9$ the TOUGH R-band data probe the rest-frame optical, and for these hosts we obtained data in bluer filters with TNG/LRS, Keck/LRIS, GTC/OSIRIS, and Gemini-S/GMOS, or used archival data. A log of the data is shown in Table 1. In addition, for the fields of GRBs 050803 and 050922B (two GRBs with uncertain redshifts), we succeeded in obtaining multi-band data (Table 1) probing the spectral energy distribution (SED) from the rest-frame UV to the near-IR (NIR). Their *Spitzer* observations are described in detail in Perley et al. (2015a, 2015b).

Table 1
Log of GRB Host Observations

GRB	Telescope Instrument	Filter	Date	Exposure Time (s)
050525A	GTC/OSIRIS	g'	2012 Aug 22	24 × 240
050730	*HST*/ACS	*F775W*	2010 Jun 10	7844
050803	GTC/OSIRIS	g'	2014 Jul 21	6 × 360
050803	Keck/LRIS	g'	2011 Aug 28	4 × 200
050803	Keck/LRIS	R	2011 Aug 28	4 × 170
050803	Keck/ESI	R	2005 Aug 04	2 × 180
050803	GTC/OSIRIS	i'	2014 Jul 21	15 × 120
050803	*HST*/WFC3	*F160W*	2011 Sep 03	906
050803	*Spitzer*/IRAC	3.6 μm	2013 Jan 31	54 × 100
050803	*Spitzer*/IRAC	4.5 μm	2013 Jan 31	54 × 100
050824	TNG/LRS	B	2010 Oct 13	2 × 900
051016B	Gemini-S/GMOS	g'	2014 Feb 07	4 × 100
051117B	Gemini-S/GMOS	u'	2014 Jan 30	9 × 60
050904	*HST*/ACS	*F850LP*	2005 Sep 26	4216
050908	*HST*/ACS	*F775W*	2010 Oct 31	7892
050922B	Keck/LRIS	g'	2008 Aug 03	2 × 360
050922B	GTC/OSIRIS	i'	2014 Jul 22	20 × 120
050922B	GTC/OSIRIS	z'	2014 Jul 22	30 × 60
050922B	*Spitzer*/IRAC	3.6 μm	2013 Aug 30	54 × 100
050922B	*Spitzer*/IRAC	4.5 μm	2013 Aug 30	54 × 100
060115	*HST*/ACS	*F814W*	2010 Aug 27	7910
060218	SDSS	u'	2004 Sep 21	...
060522	*HST*/ACS	*F110W*	2010 Oct 17	8395
060526	*HST*/ACS	*F775W*	2009 Aug 09	7844
060605	*HST*/ACS	*F775W*	2010 Oct 06	7862
060607A	*HST*/ACS	*F775W*	2010 Sep 17	7910
060729	Gemini-S/GMOS	g'	2008 Jan 29	15 × 180
060805A	Keck/LRIS	g'	2008 Feb 12	1080
060912	TNG/LRS	B	2010 Oct 13	2 × 150
060927	*HST*/WFC3	*F110W*	2010 Sep 25	13992
061021	Keck/LRIS	g'	2007 Dec 13	560
061110A[a]	Keck/LRIS	V	2006 Nov 21	680
061110B	*HST*/ACS	*F775W*	2010 Sep 23	7862
070721B	*HST*/ACS	*F775W*	2010 Nov 13	7844

Note.
[a] The observation was performed 21 days after the GRB. The afterglow was very faint so that only the accompanying GRB-SN could contaminate the host measurement. However, GRB-SNe have a red spectrum and the observed bandpass probed the rest-frame u' band, which makes any contamination unlikely.

To secure the field calibration of GRB 060805A we used the 60 inch Palomar telescope, and for GRB 060729 we used the Gamma-ray Optical/Near-infrared Detector (GROND; Greiner et al. 2008) mounted at the MPG/ESO 2.2 m telescope.

Furthermore, we incorporated measurements reported in the literature; specifically we used Perley et al. (2009) for GRB 050416A, Chen et al. (2009) for 050820A, Hjorth et al. (2012) for the K_s band photometry for GRBs 050803 and 050922B, Mangano et al. (2007) for 060614, Krühler et al. (2011) for 070306, and Tanvir et al. (2012) for GRBs 050904, 060522, and 060927.

The ground-based data were reduced in a standard fashion (bias subtraction, flat fielding, co-adding) with dedicated software packages (Keck: customized IDL routine, Gemini:

Gemini IRAF package GROND: customized pipeline (for details see Krühler et al. 2008; Yoldaş et al. 2008), and all other data with IRAF; Tody 1986). *HST* observations, after standard "on-the-fly" processing, were subsequently cleaned for bias striping, introduced due to the replacement electronics after Servicing Mission 4 (2009 May 11–24), and then drizzled with the multidrizzle software (Koekemoer et al. 2003) into final science images. The reduction of the *Spitzer* data is described in Perley et al. (2015b).

3. METHODS

3.1. Photometry

The photometry for the ground-based images was performed as described in D. Malesani et al. (2015, in preparation): if a host was detected at $>5\sigma$ confidence level, we chose a sufficiently large aperture to measure the total flux. For hosts detected at a lower confidence level, we reduced the radius to the stellar FWHM and applied an aperture correction derived from the brighter hosts in the sample.

Once an instrumental magnitude was established it was photometrically calibrated against zeropoints (GRB 051117B), against the brightness of a photometric standard star (GRB 050525A), a number of field stars measured in a similar way (GRBs 060729), or tied to the SDSS DR8 (the rest; Aihara et al. 2011). In some cases, we converted the SDSS photometry into the Bessel system using Lupton,[15] if needed. These measurements were finally corrected for Galactic extinction using the extinction maps by Schlegel et al. (1998) and transformed into the AB system using Blanton & Roweis (2007) and Breeveld et al. (2011). These magnitudes are listed in Table 2.

The *R*-band observation of the host galaxy of GRB 050502B is affected by Lyα absorption in the host galaxy and in the intergalactic medium (IGM). To quantify this attenuation, we compared the observed to the expected $(R-I)$ color of the afterglow. Afonso et al. (2011) reported that the X-ray-to-optical SED of the afterglow can be described by a simple power law, $F_\nu \propto \nu^{-\beta}$, with a spectral index of $\beta \sim 0.9$. For this model, the expected $(R-I)_{\rm AB}$ color is 0.22 mag, i.e., the emission received in the *R* band is dimmed by 0.95 mag, assuming no reddening at the GRB site. Throughout the paper we assume that the host galaxy has the same attenuation. The values reported in Table 2 include this correction.

For the *HST* images we measured the background-subtracted flux within an aperture with a radius of $0\farcs25$. To quantify the measurement error, we randomly distributed 40 apertures of the same radius within $3''$ from the optical afterglow. These apertures had a minimum distance of $0\farcs6$ from any object to avoid source contamination. After that, we computed the standard deviation as a proxy for the photometric error. To account for flux losses we applied aperture corrections that were calculated from the encircled energy (Sirianni et al. 2005). If no host was detected, we measured the 3σ limiting magnitude via $m_{\rm limit} = 23.9 - {\rm AP_{cor}} - 2.5\ \log\left(F_\nu + 3\sigma\left(F_\nu\right)\right)$ where $\rm AP_{cor}$ is the aperture correction and F_ν is the formal flux density in μJy measured at the position of the optical afterglow with its 1σ error $\sigma\left(F_\nu\right)$.

[15] http://www.sdss.org/dr5/algorithms/sdssUBVRITransform.html

At $z \sim 3$, an angular size of $0\farcs5$ translates to a physical scale of ~4 kpc. This diameter is at the lower end of the observed size distribution of LBGs (Hathi et al. 2008). Increasing the aperture radius to $0\farcs3$, the average size of an LBG at $z \sim 3$ leads to no significant increase in flux. On the contrary, the measurement would have been affected by neighboring objects if the radius exceeded $0\farcs4$.

The analysis of the *Spitzer* data is described in detail in Perley et al. (2015b); in brief, after downloading the processed PBCD images from the *Spitzer* Legacy Archive,[16] we modeled and subtracted nearby contaminating sources, and then measured the flux of the host via aperture photometry and used the IRAC handbook zeropoints to convert the instrumental to apparent magnitudes.[17]

3.2. Host Identification

D. Malesani et al. (2015, in preparation) describe in detail how the hosts were identified in the deep VLT images. The additional data obtained with ground-based telescopes have a similar spatial resolution and do not exceed the limiting magnitudes of the VLT images. In contrast the *HST* images exceed the VLT images in spatial resolution and depth (see Figure 1). This necessitates repeating the host identification. In the following we can limit the discussion to the $z = 3$–4 hosts, whereas the host identification of GRB 050820A is discussed in Chen et al. (2009) and Chen (2012), and of GRBs 050904, 060522, and 060927 in Tanvir et al. (2012).

To identify the most likely host galaxy candidate, we chose the probabilistic approach by Bloom et al. (2002) (For a detailed discussion, see also Perley et al. 2009). This method is based on the observed galaxy density from Hogg et al. (1997) and quantifies the chance probability $p_{\rm ch}$ of finding a galaxy with a certain magnitude and a certain distance from the GRBs. This chance probability is given by

$$p_{\rm ch} = 1 - \exp\left(-\pi \times r_{\rm eff} \times \sigma(m)\right)$$

where $r_{\rm eff}$ is the effective radius and $\sigma(m)$ is the galaxy density for a given observed magnitude m. The effective radius depends on the half-light radius $r_{1/2}$, the distance from the GRB r_0, and the localization accuracy. The localization accuracy is defined by the error of aligning the *Hubble Space Telescope* (*HST*) images to images of the optical afterglows, which is between $0\farcs033$ and $0\farcs061$. The effective radius in Bloom et al. (2002) can hence be re-written as $r_{\rm eff} = 2\ r_{1/2}$ if $r_0 < r_{1/2}$ and $r_{\rm eff} = (r_0^2 + 4\ r_{1/2}^2)^{1/2}$ if $r_0 > r_{1/2}$. The half-light radii were measured with SExtractor v2.19.5 (Bertin & Arnouts 1996). To limit the number of candidates we set an upper limit of $3''$ on the GRB offset and required a chance probability of $p_{\rm ch} < 5\%$.

The final candidates are listed in Table 3 (not corrected for Galactic reddening, whereas the unreddended magnitudes are reported in Table 2). The host offsets are consistent with the observed distribution for the TOUGH sample (D. Malesani et al. 2015, in preparation). If no host candidate was detected, we report the nominal flux and the 3σ limiting magnitude. The host identifications of GRBs 060115 and 060605 are not unique, where alternative candidates for each of these GRBs

[16] http://sha.ipac.caltech.edu/applications/Spitzer/SHA/

[17] http://irsa.ipac.caltech.edu/data/SPITZER/docs/irac/iracinstrumenthandbook/

Table 2
UV Properties of the TOUGH Sample

GRB	Redshift[a]	Filter	m (mag)	$\beta_{\rm UV}$	$M_{1600\,\text{Å}}$[b] (mag)	GRB	Redshift	Filter	m (mag)	$\beta_{\rm UV}$	$M^{\rm b}_{1600\,\text{Å}}$ (mag)
Hosts with Known Redshifts											
050315	1.95	*R*	24.51 ± 0.15	-1.54 ∓ 0.03	-20.08 ± 0.14	060707	3.42	*R*	25.01 ± 0.06	-1.62 ∓ 0.01	-20.82 ± 0.06
050318	1.444	*R*	>26.95	<-1.92	>-17.16	060708	1.92 ± 0.12	*R*	26.94 ± 0.28	-1.89 ∓ 0.03	-17.75 ± 0.27
050401	2.898	*R*	26.19 ± 0.31	-1.79 ∓ 0.04	-19.31 ± 0.31	060714	2.71	*R*	26.46 ± 0.28	$-1.82^{-0.03}_{+0.04}$	-18.91 ± 0.28
050406	$2.7^{+0.29}_{-0.41}$	*R*	26.76 ± 0.34	-1.86 ∓ 0.04	-18.60 ± 0.34	060719	1.53	*R*	24.81 ± 0.12	-1.64 ∓ 0.02	-19.27 ± 0.11
050416A	0.653	g'	24.00 ± 0.03	-1.73 ∓ 0.01	-18.26 ± 0.03	060729	0.54	g'	25.30 ± 0.16	-1.92 ∓ 0.02	-16.66 ± 0.15
050502B[c]	5.2 ± 0.3	*R*	>25.98	<-1.85	>-20.61	060805A[e]	0.60	g'	24.61 ± 0.07	-1.83 ∓ 0.01	-17.53 ± 0.06
050525A	0.606	g'	>25.83	<-1.95	>-16.40	060805A[e]	2.36	*R*	25.26 ± 0.14	-1.65 ∓ 0.02	-19.79 ± 0.13
050714B	2.438	*R*	25.51 ± 0.20	-1.69 ∓ 0.03	-19.61 ± 0.19	060814	1.92	*R*	22.96 ± 0.11	-1.19 ∓ 0.03	-21.46 ± 0.10
050730	3.969	*F775W*	>27.50	<-1.98	>-18.58	060908	1.88	*R*	25.66 ± 0.18	-1.74 ∓ 0.03	-18.93 ± 0.17
050801	1.38 ± 0.07	*R*	>26.74	<-1.91	>-17.26	060912A	0.94	*B*	22.59 ± 0.06	$-1.33^{-0.01}_{+0.02}$	-20.39 ± 0.06
050819	2.504	*R*	23.99 ± 0.09	-1.39 ∓ 0.02	-21.13 ± 0.09	060923A[f]	$2.47^{+0.33}_{-0.52}$	*R*	26.12 ± 0.24	-1.78 ∓ 0.03	-19.05 ± 0.23
050820A	2.615	*F775W*	26.30 ± 0.06	-1.80 ∓ 0.01	-18.96 ± 0.06	060923B	1.51	*R*	24.15 ± 0.16	-1.53 ∓ 0.03	-19.83 ± 0.14
050822	1.434	*R*	24.36 ± 0.08	-1.59 ∓ 0.01	-19.54 ± 0.07	060927	5.46	*F110W*	>28.23	<-2.10	>-18.39
050824	0.828	*B*	24.11 ± 0.16	-1.67 ∓ 0.03	-18.71 ± 0.15	061007	1.26	*R*	24.56 ± 0.17	-1.65 ∓ 0.03	-19.08 ± 0.15
050904	6.295	*F850LP*	>26.27	<-1.95	>-20.58	061021	0.35	g'	26.40 ± 0.16	-2.07 ∓ 0.01	-14.65 ± 0.15
050908	3.347	*F775W*	$27.55^{+0.30}_{-0.24}$	-1.96 ∓ 0.03	$-18.22^{+0.30}_{-0.24}$	061110A	0.76	*V*	25.25 ± 0.10	-1.85 ∓ 0.01	-17.41 ± 0.09
050915A	2.527	*R*	24.70 ± 0.16	-1.54 ∓ 0.03	-20.47 ± 0.15	061110B	3.43	*F775W*	$27.02^{+0.26}_{-0.21}$	$-1.91^{-0.03}_{+0.02}$	$-18.79^{+0.26}_{-0.21}$
050922C	2.199	*R*	>26.29	<-1.81	>-18.64	061121	1.32	*R*	22.84 ± 0.03	-1.31 ∓ 0.01	-20.67 ± 0.03
051001	2.43	*R*	24.53 ± 0.13	-1.51 ∓ 0.03	-20.55 ± 0.12	070103	2.62	*R*	24.21 ± 0.14	-1.43 ∓ 0.03	$-21.03^{+0.13}_{-0.14}$
051006	1.059	*R*	23.03 ± 0.07	-1.43 ∓ 0.01	-20.03 ± 0.06	070110	2.35	*R*	25.19 ± 0.11	-1.64 ∓ 0.02	-19.84 ± 0.11
051016B	0.936	g'	23.13 ± 0.03	-1.46 ∓ 0.01	-19.87 ± 0.03	070129	2.34	*R*	24.23 ± 0.12	-1.45 ∓ 0.03	-20.75 ± 0.11
051117B	0.481	u'	22.91 ± 0.19	-1.65 ∓ 0.03	-18.67 ± 0.18	070224	1.99	*R*	26.02 ± 0.31	-1.78 ∓ 0.04	$-18.71^{+0.30}_{-0.29}$
060115	3.533	*F814W*	$27.21^{+0.27}_{-0.21}$	-1.94 ∓ 0.03	-18.65 ± 0.27	070306	1.50	g'	22.90 ± 0.09	-1.18 ∓ 0.03	-21.21 ± 0.09
060218	0.034	u'	20.61 ± 0.12	-2.02 ∓ 0.01	-15.20 ± 0.11	070318	0.84	*R*	24.60 ± 0.11	-1.76 ∓ 0.01	-18.18 ± 0.10
060306[d]	1.559	*R*	24.21 ± 0.08	-1.54 ∓ 0.02	-19.86 ± 0.07	070328	2.06	*R*	24.55 ± 0.13	-1.54 ∓ 0.03	-20.17 ± 0.12
060522	5.11	*F110W*	>27.82	<-2.05	>-18.69	070419B	1.96	*R*	25.20 ± 0.20	-1.66 ∓ 0.03	-19.44 ± 0.19
060526	3.221	*F775W*	>27.52	<-1.95	>-18.18	070506	2.31	*R*	26.21 ± 0.22	-1.79 ∓ 0.03	-18.83 ± 0.21
060604	2.136	*R*	25.62 ± 0.18	-1.71 ∓ 0.03	-19.23 ± 0.17	070611	2.04	*R*	>27.27	<-1.92	>-17.55
060605	3.773	*F775W*	$27.48^{+0.40}_{-0.29}$	-1.97 ∓ 0.03	$-18.50^{+0.40}_{-0.29}$	070721B	3.63	*F775W*	$27.69^{+0.47}_{-0.33}$	$-1.99^{-0.04}_{+0.03}$	$-18.22^{+0.47}_{-0.33}$
060607A	3.075	*R*	>28.05	<-1.99	>-17.57	070802	2.45	*R*	25.25 ± 0.21	-1.64 ∓ 0.04	-19.88 ± 0.20
060614	0.125	*u*	24.71 ± 0.30	-2.10 ∓ 0.01	-14.06 ± 0.29						
Hosts with Unknown Redshifts[g]											
050726	3.5	*R*	>26.19	<-1.81	>-19.68	061004	3.5	*R*	>25.84	<-1.76	>-20.03
050803	3.5	i'	26.29 ± 0.50	$-1.83^{-0.06}_{+0.07}$	-19.55 ± 0.50	070330	3.5	*R*	>26.19	<-1.81	>-19.67
050922B	3.5	i'	25.20 ± 0.15	-1.67 ∓ 0.03	-20.63 ± 0.15	070621	3.5	*R*	25.85 ± 0.23	$-1.77^{-0.03}_{+0.04}$	-20.02 ± 0.23
060919	3.5	*R*	25.80 ± 0.26	-1.76 ∓ 0.04	-20.07 ± 0.26	070808	3.5	*R*	26.85 ± 0.33	-1.90 ± 0.04	-19.01 ± 0.33
060923C	3.5	*R*	25.49 ± 0.18	-1.71 ∓ 0.03	-20.38 ± 0.18						
New Photometric Redshifts[h]											
050803	3.5 ± 0.5	i'	26.29 ± 0.5	$-1.83^{-0.06}_{+0.07}$	-19.55 ± 0.50	050922B	4.5 ± 0.5	i'	25.20 ± 0.15	-1.69 ∓ 0.03	-21.13 ± 0.15

Notes. All magnitudes are corrected for Galactic extinction and were converted into the AB system. For the non-detections we report the 3σ limiting magnitudes. Redshifts were taken from Hjorth et al. (2012), Perley et al. (2013), and Krühler et al. (2015).

[a] For hosts with photometric redshifts, we report the values at the nominal redshifts.

[b] The absolute magnitude was computed through $M_{1600\,\text{Å}} = m - \text{DM}(z) - 2.5(\beta_{\text{UV}} + 2)\log\left((1+z)1600\,\text{Å}/\lambda_{\text{obs}}\right) + 2.5\ \log(1+z)$ where DM is the distance modulus for the assumed cosmology.

[c] Luminosity includes a correction for IGM and Lyα absorption.

[d] The Hα emission line is double peaked with the centers of the peaks at $z = 1.5585$ and $z = 1.5597$. Without loss of generality we assume $z = 1.559$.

[e] The host identification is not unique.

[f] The redshift range of 060923A was constructed by combining limits from Jakobsson et al. (2012) and Perley et al. (2013).

[g] For hosts with redshift limits, we report the UV properties at $z = 3.5$. For the hosts of GRBs 060919, 060923C, 070621, and 070808, the luminosities are strictly speaking upper limits. Note, the redshift of 060923C is between $z = 0.86$ and $z = 3.5$. For GRBs 050726 ($z < 5.5$), 050803 ($z < 6.1$), 050922B ($z < 6.1$), 061004 ($z < 10$), and 070330 ($z < 5.5$) we report their luminosities at $z = 3.5$ to avoid corrections for IGM and Lyα absorption.

[h] Listed are the two hosts for which new redshift constraints were obtained through SED fitting. As discussed in Section 3.3 a broad range of physical galaxy parameters and redshifts fits the data within their uncertainties. The likely redshift of GRB 050803 is $z \sim 3.5$ and of GRB 050922B $z \sim 4.5$.

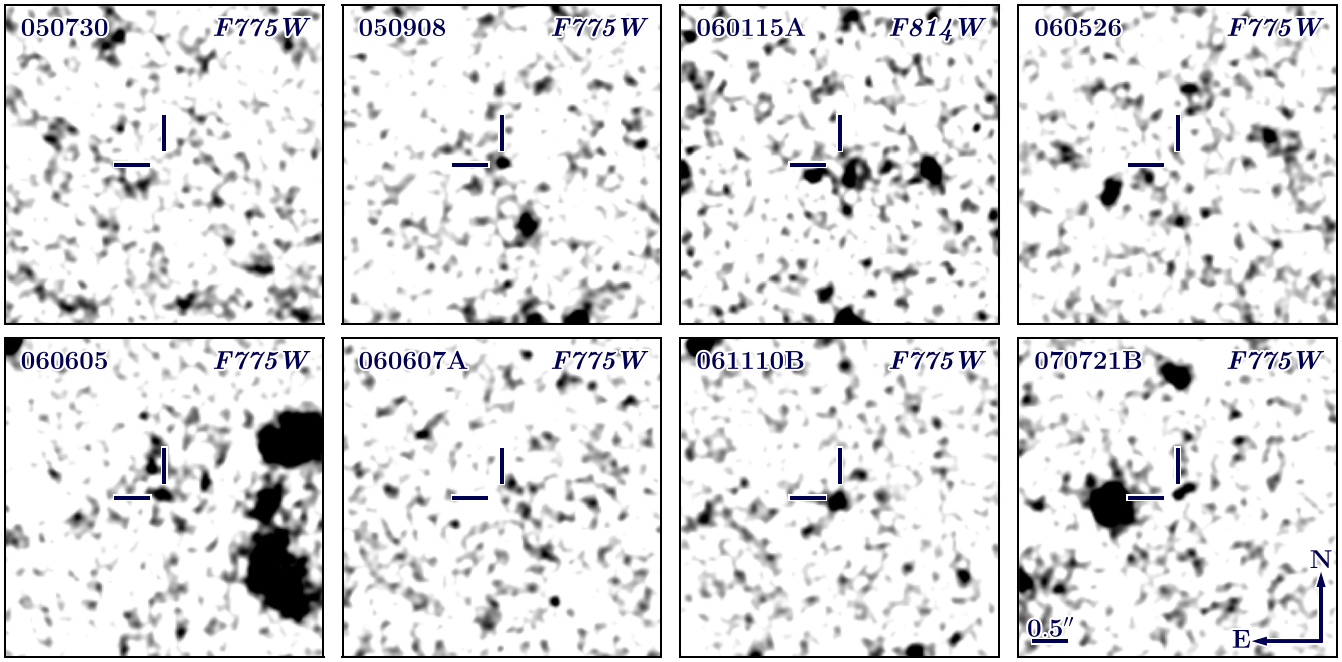

Figure 1. Poststamps of the fields recently observed with *HST*/ACS. Each cutout has a size of 5″ × 5″, corresponding to ∼37.3 × 37.3 kpc^2 at $z = 3.5$. The blue crosshairs mark the positions of optical afterglow. About 1″ east of the afterglow of GRB 070721B is a galaxy with $m(F775W) \sim 24.4$ mag ($p_{\rm ch} \sim 2\%$). In Schulze et al. (2012), we showed that this galaxy is in fact the galaxy counterpart of the intervening DLA at $z = 3.0939$ reported in Fynbo et al. (2009). For presentation purposes all images were smoothed with a Gaussian kernel with a width of 0.″05.

Table 3
Properties of the $z = 3$–4 Host Galaxies Observed With *HST*

GRB	α, δ (J2000)	$r_{1/2}$ (″)	r_0 (″)	Band	F_ν (nJy)	Brightness (mag)	$p_{\rm ch}$
050730	⋯	⋯	⋯	*F775W*	7 ± 7	>27.6	⋯
050908	01:21:50.727, −12:57:17.31	0.05	0.02	*F775W*	29 ± 7	$27.60^{+0.30}_{-0.24}$	0.002
060115	03:36:08.314, +17:20:42.80	0.09	0.28	*F814W*	38 ± 7	$27.27^{+0.22}_{-0.18}$	0.020
	03:36:08.351, +17:20:42.86	0.08	0.44	*F814W*	26 ± 7	$27.68^{+0.34}_{-0.26}$	0.052
060526	⋯	⋯	⋯	*F775W*	5 ± 7	>27.66	⋯
060605	21:28:37.312, −06:03:30.96	0.09	0.06	*F775W*	30 ± 9	$27.55^{+0.38}_{-0.28}$	0.007
	21:28:37.321, −06:03:30.56	0.06	0.47	*F775W*	28 ± 9	$27.63^{+0.42}_{-0.30}$	0.054
060607[a]	⋯	⋯	⋯	*F775W*	13 ± 8	>27.48	⋯
061110B	21:35:40.396, +06:52:34.30	0.12	0.05	*F775W*	45 ± 10	$27.10^{+0.26}_{-0.21}$	0.008
070721B	02:12:32.935, −02:11:40.63	0.08	0.20	*F775W*	25 ± 9	$27.76^{+0.47}_{-0.33}$	0.018

Note. For each galaxy we list its half-light radius $r_{1/2}$, its projected distance to the GRB r_0, its flux density F_ν, and the apparent magnitude. If no host candidate was detected, we report the nominal flux density at the afterglow position and the corresponding 3σ limiting magnitude. All magnitudes (but not the flux densities) include an aperture correction but *no* correction for Galactic reddening. The uncertainty in the reported coordinates is ∼0.″4 (comprising the astrometry error of the optical afterglow images and the alignment error of the VLT and *HST* images). See Section 3.2 for details.

[a] There is in fact a host candidate with a chance probability of $p_{\rm ch} = 0.04$ 0.″29 from the afterglow. However, it is only detected in a very small aperture with a radius of 0.″2. The coordinates of the object are R.A., decl.(J2000) = 21:58:50.388, −22:29:46.68 ± 0.″4. Its magnitude is $m(F775W) = 28.28^{+0.53}_{-0.35}$ mag.

have the same magnitudes within 2σ. For simplicity, we used their weighted means in the further analysis.

3.3. Photometric Redshifts

Although the TOUGH sample has a current redshift completeness of 87%, nine hosts remain without precise redshift information (Table 2). We succeeded in obtaining multi-band data for GRBs 050803 and 050922B from 4000 to 42000 Å (Table 1) to model their SEDs and obtain photometric redshifts.

The field of GRB 050803 was observed in the same filters but with a different telescope (Table 2). We built super-stacks for each band by resampling these data to the grid of the Keck/LRIS images (which has the highest spatial resolution) while

Table 4
Broad-band Photometry of 050803 and 050922B

GRB 050803		GRB 050922B	
Band	Brightness (mag)	Band	Brightness (mag)
g'	>27.45	g'	27.50 ± 0.50
R	26.29 ± 0.22	R	26.52 ± 0.22
i'	26.45 ± 0.50	i'	25.18 ± 0.14
F160W	25.74 ± 0.18	z'	25.01 ± 0.34
K_s	>23.30	K_s	>24.00
3.6 μm	>24.67	3.6 μm	24.77 ± 0.36
4.5 μm	>25.00	4.5 μm	24.60 ± 0.46

Note. All magnitudes are corrected for Galactic reddening. Non-detections are reported at 3σ confidence level. The *K*-band photometry was taken from Hjorth et al. (2012).

conserving the flux and weighting the images by their limiting magnitudes. The final extinction-corrected magnitudes of the two hosts are reported in Table 4.

We modeled the SED with `Le Phare` (Arnouts et al. 1999; Ilbert et al. 2006),[18] using a grid of galaxy templates based on Bruzual & Charlot (2003) stellar population-synthesis models with the Chabrier IMF and a Calzetti dust attenuation curve (Calzetti et al. 2000). For a description of the galaxy templates, physical parameters of the galaxy fitting, and their error estimation, we refer to Krühler et al. (2011). To account for zeropoint offsets in the cross calibration and absolute flux scale, a systematic error contribution of 0.05 mag was added in quadrature to the uncertainty introduced by photon noise. Figure 2 displays the observed host SEDs and their best fits.

Considering the brightness of the two galaxies ($R > 26$ mag) and their measurement errors, this fitting does not yield a unique redshift solution for either of the two galaxies. A broad range of physical galaxy parameters and redshifts fit the data within their uncertainties. Of particular interest in our case is the possibility that the galaxies are at $z > 3$. A high redshift does in fact provide a good description of the photometry in both cases. The SED of the host of GRB 050922B has significant $g' - r'$ and $r' - i'$ colors which are reasonably well explained by the Lyα and Lyman-limit breaks at $z \sim 4.5$. Similarly, the red $g' - r'$ and blue $r' - i'$ colors of the galaxy hosting GRB 050803 is indicative of a redshift of $z \sim 3.5$. Lower redshift solutions ($z < 1$) exist as well in both cases, but based on the available photometry, it is at least plausible that both GRBs originated at $z > 3$.

3.4. The Obscured UV Luminosity

Although we have at least one measurement of the rest-frame UV continuum between 1216 and 4000 Å for each host galaxy in our sample, these data probe different parts of the UV continuum; on average they probe the rest-frame at 2140 Å. UV LFs of LBG samples are typically reported at 1500–1700 Å (e.g., Arnouts et al. 2005; Reddy & Steidel 2009; Oesch et al. 2010; Bouwens et al. 2014). To shift the UV luminosities of the TOUGH sample to the common rest-frame at 1600 Å, a *K*-correction was applied assuming the UV continuum to be power-law shaped ($F_\lambda \propto \lambda^{-\beta_{\rm UV}}$). However, LBG surveys have also shown that the spectral slope is luminosity and redshift dependent (e.g., Bouwens et al. 2009, 2010b). To account for that we make use of the parameterization by Trenti et al. (2014) that is based on the findings for LBGs by (Bouwens et al. 2012, and references therein). Since the slope depends on the unknown observed UV luminosity, we solve the inverse problem: we compute the expected apparent magnitudes for a range of UV luminosities (-30 mag $< M < -8$ mag) at the redshift of each GRB and select the luminosity that minimizes the difference between the observed and the expected apparent magnitudes. In Table 2 we summarize the best-fit slopes and luminosities.

We note that the UV luminosities in the FUV are highly sensitive to any reddening correction. In LBG surveys it is a common practice to build the LF from the obscured UV luminosities, and therefore without any loss of generality or limitation in the comparison with LBG surveys, we omit any reddening correction.

[18] http://www.cfht.hawaii.edu/~arnouts/LEPHARE

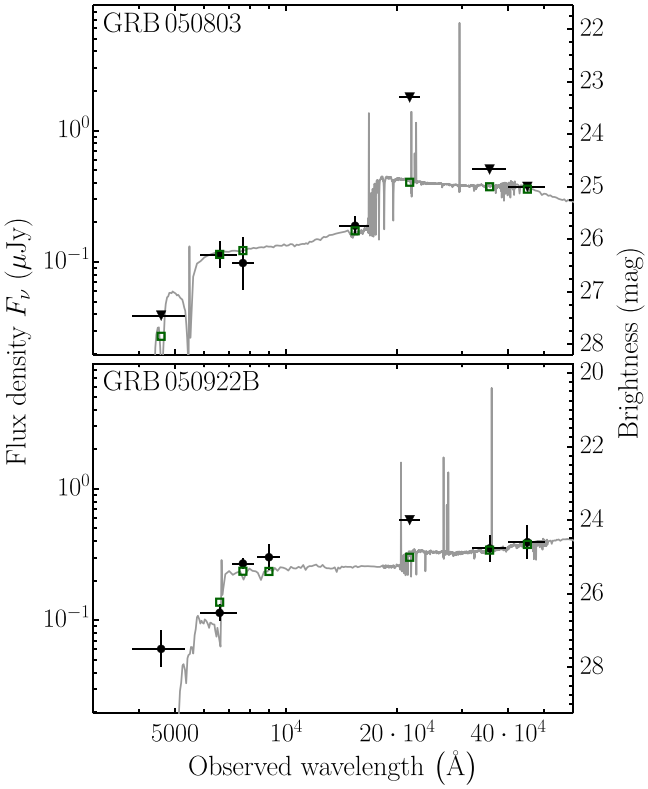

Figure 2. Spectral energy distributions (SEDs) of GRBs 050803 and 050922B and their fits. The solid line displays a fit of the SED with Le Phare. The green open squares are the model predicted magnitudes. Given the sampling and the measurement errors, a broad range of physical galaxy parameters and redshifts fits the data within their uncertainties. Assuming the two galaxies to be star-forming, the most likely redshift of GRB 050803 is between $z = 3$ and 4 and of GRB 050922B between $z = 4$ and 5. See Section 3.3 for details.

3.5. The Impact of the UV Slope on the K-correction

The exact shape of the unobscured UV continuum is determined by the age of the young stellar population and metallicity. Savaglio et al. (2009, and the update in the GHostS database) and Perley et al. (2013) showed that the observed age distribution extends from a few tens of megayears to two billion years. Though this result is based on heterogeneous samples, the maximum age is consistent with limits we extracted from the TOUGH sample (D. Malesani et al. 2015,

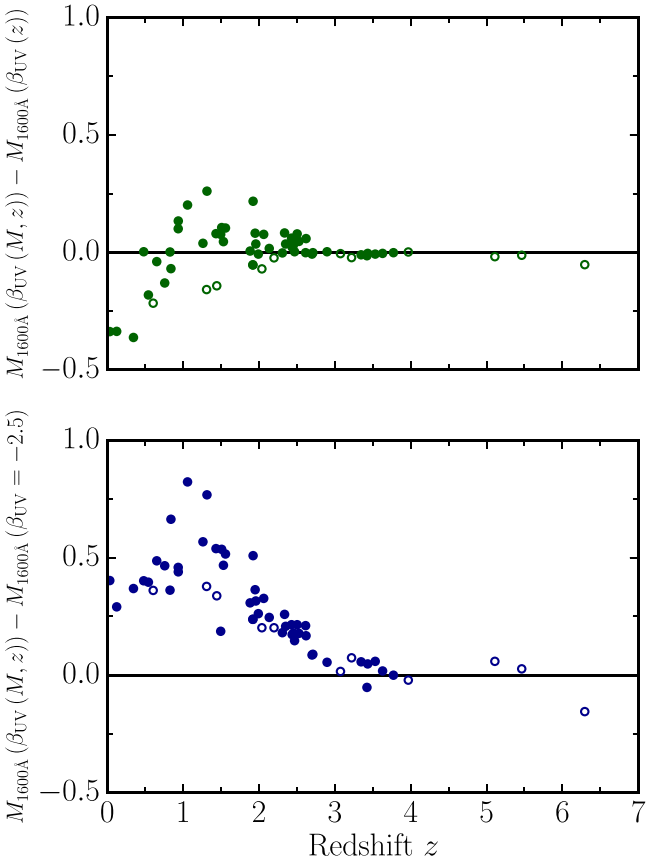

Figure 3. Impact of the approximations on the rest-frame UV continuum on the observed UV luminosity at 1600 Å. The continuum is assumed to be power-law shaped with $F_\lambda \propto \lambda^{-\beta_{UV}}$, where the slope can be luminosity and redshift dependent. Top panel: luminosity- and redshift-dependent slope vs. luminosity-independent but redshift-dependent slope. Bottom panel: luminosity- and redshift-dependent slope vs. uniform slope. Detected hosts are displayed as filled circles and non-detected hosts as open circles. For clarity, we only show the hosts with known redshifts. We omit the host of GRB 050502B because of its uncertain IGM correction. The size of the average error is shown in the top panel.

in preparation). To check whether the slopes used in our analysis are consistent with these ages, we fit the UV continuum of single-age stellar population models from Bruzual & Charlot (2003) between 1350 and 3600 Å with power-law models. We find that the slopes vary between $\beta_{UV} \sim -2.8$ and ~3.5 for ages between 0.005 and 2.5 Gyr, in agreement with the values derived in Section 3.4.

We next assess how the assumption about the luminosity and redshift dependence affects our results. We first assume the slope to be luminosity independent. We constrain the redshift evolution using results from Schiminovich et al. (2005), Finkelstein et al. (2012), and Hathi et al. (2013). Between $z = 0$ and $z = 8$, the UV slope could be parameterized as

$$\beta_{UV}(z) = (-1.62 \pm 0.04) + (-0.07 \pm 0.01) \times z \quad (1)$$

for luminosities between ~0.1 $L_\star$ and ~1.5 $L_\star$. Figure 3 (top panel) displays the difference in the observed luminosity for the different parameterizations of the UV slope. The median difference is 0.01 mag and in most cases negligible. The largest differences of 0.26 mag are observed at $z \sim 1$ where the *R*-band data have the largest distance from the common rest frame at 1600 Å.

Next we drop the redshift dependency and assume a very young stellar population with a characteristic spectral slope of $\beta_{UV} = -2.5$ for all hosts. The luminosity will increase for all hosts (Figure 3, bottom panel). The largest shift of 0.82 mag is observed at $z \sim 1$. However, it is very unlikely that the majority of GRB hosts have such blue UV continua. Several low-redshift hosts are known to have evolved young stellar populations, e.g., GRB 970228 ($z = 0.695$): age = 1.7 Gyr; GRB 990712 ($z = 0.433$): age = 1.1 Gyr; and GRB 011121 ($z = 0.362$): age = 2.3 Gyr (Savaglio et al. 2009). In conclusion, though individual hosts may be more or less luminous than inferred from our ansatz, we do not consider our UV slope assumptions to have any systematic effect on the ensemble above $z \sim 1$.

4. RESULTS

4.1. GRB Host Luminosity Distribution

Figure 4 (left panel) plots the absolute magnitudes at 1600 Å (detections and upper limits) of the sample GRB hosts versus redshift. The absolute magnitudes of the detected hosts span a wide range in magnitude from −14 to −21.4 mag. The majority of the upper limits on non-detected hosts are as deep as, and deeper than, any of the host detections, particularly at high redshift ($z > 3$). All upper limits, except for one host at $z = 6.295$, are well below the median magnitude of the detected sample.

It is interesting to note that the brightest hosts, i.e., those above the median absolute magnitude, span a quite limited redshift range between $z \sim 1$ and $z \lesssim 3$. Conversely the dimmest 50% of hosts (detections and upper limits) span the entire redshift range of the sample. This evolution is similar to that of the UV-inferred global star formation rate density (e.g., Daddi et al. 2007; Noeske et al. 2007; Rodighiero et al. 2010; Elbaz et al. 2011; Bouwens et al. 2014), which also peaks at $z = 2$–3.

Above $z > 3$, there is a conspicuous absence of any host detection above the median magnitude, except for the single bright $M_{1600\,Å} = -20.8$ mag host (GRB 060707) at $z = 3.424$, though the host of GRB050922B could have similar luminosity (for details see Section 3.3). At the other end of the redshift scale, below $z \sim 1$, there are once again no hosts above the median magnitude. Our unbiased host sample seems to suggest that GRBs favor lower luminosity hosts throughout the entire redshift range in which they are detected and are only found in UV brighter hosts in the range between $1 < z < 3$, though we note (as discussed below) that some of the hosts with unknown redshifts may in reality exist in the higher redshift range.

Figure 5 plots the rate density (number per unit comoving volume per year) of TOUGH GRBs occurring in hosts above and below the overall survey median luminosity (dotted line left panel Figure 4) versus redshift. Although the overall numbers are small, the volume density of the brighter host fraction is lower than that of the fainter fraction at all redshifts except $1 < z < 3$ where bright hosts reverse this trend to become 2.5–3 times more common than those below the global median. We caution that the relatively low numbers in each large and somewhat arbitrary redshift bin prevent any firmer statistical conclusion from being drawn from the binned data. Further analysis of the cumulative distribution function (CDF) of the TOUGH hosts compared to model LFs derived from

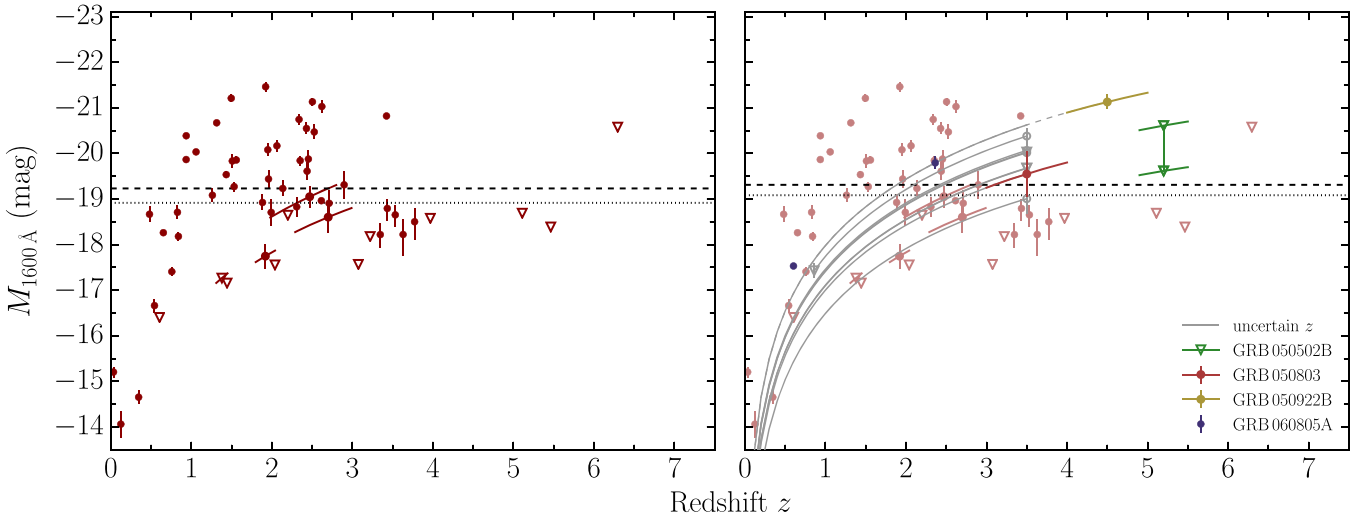

Figure 4. Absolute magnitudes of our GRB host galaxy sample plotted vs. redshift. Left: host with known redshifts of detected (•) and non-detected hosts (▽). The horizontal dashed line indicates the median luminosity of detected hosts (being −19.2 mag) and the dotted line of all including the non-detected hosts (the median value being −18.9 mag). Right: location of the hosts with uncertain redshifts (curved lines), GRB 060805A, which does not have a unique host identification, and GRB 050502B, which has an uncertain IGM correction. To illustrate the impact of the IGM correction, the parameter space ranging from no IGM correction to the conservative IGM correction discussed in Section 2.2 is shown. As in the left panel, the dashed line indicates the median luminosity of detected hosts (being −19.3 mag) and the dotted line of all hosts (being −19.1 mag), where we assumed hosts without redshift information to be at $z = 3.5$ according to Table 2. For GRBs 050803 and 050922B, the likely redshift ranges from the SED modeling are highlighted. (see Section 3.3 for details). Because of the ambiguity of the redshift ranges, we also show their tracks if they are at lower redshifts.

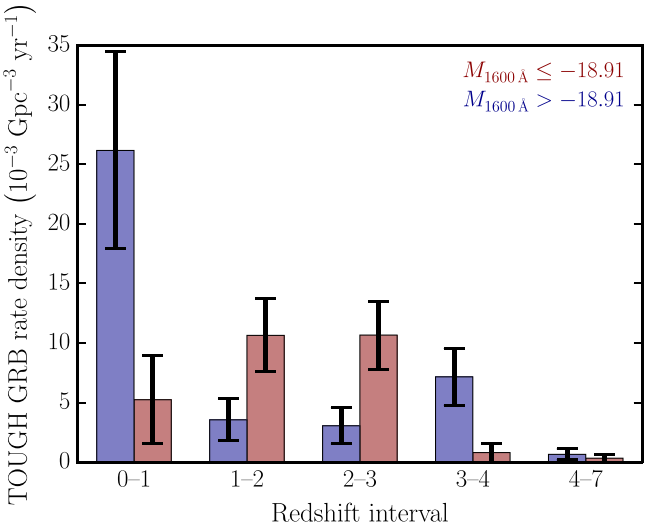

Figure 5. GRB rate density (normalized to the TOUGH period of 2.5 years; Hjorth et al. 2012) in hosts below and above the median UV luminosity of the TOUGH sample. For simplicity only hosts with known redshifts are shown. GRBs occur in faint hosts at $z < 1$ about a factor of five times more frequently, while at $z = 1$–3, bright hosts are factor of 2.5–3 times more common than faint hosts. Error bars represent Poisson errors on each bin. For details see Section 4.1.

LBG populations in Section 4.3 investigates these preliminary observations in greater detail.

In the following sections, we investigate how GRB hosts trace the SFR history, in particular whether they follow the model proposed by Fynbo et al. (2002, see also Jakobsson et al. 2005) of GRBs selecting galaxies from a general population according to their SFR or whether an additional dependency must be invoked, such as metallicity (Stanek et al. 2006; Modjaz et al. 2008; Levesque et al. 2010).

We note that the redshifts of nine hosts are uncertain (Table 2) within defined limits (for details see Jakobsson et al. 2012), one host identification (GRB 060805A) is non-unique, and the IGM correction for one host (GRB 050502B) is uncertain. In the right panel of Figure 4 we plot their possible positions in the $M_{1600\,\text{Å}}$–z plane (gray lines for hosts of uncertain z, green data points for the host with uncertain IGM correction, and blue data points for the non-unique host identification), where it can be seen that the plausible distribution of these uncertain hosts shows no discrepancy from the firm detections/limits. We discuss further the effects of these unknown redshift hosts on our results in Section 5.1.

4.2. The Evolution of the Median UV Luminosity

As a first diagnostic to investigate whether GRBs are biased or unbiased tracers of star formation, we investigate the evolution of the median obscured UV luminosity of the hosts. Recently Trenti et al. (2014) presented tracks for the evolution of the median observed UV luminosity of GRB host galaxies for various levels of GRB production bias with respect to host metallicity, characterized by a parameter p which represents a minimum, metal-independent plateau for the efficiency of forming a GRB. Thus a low value of p characterizes a high level of bias toward low metallicity hosts ($p = 0$ representing a stringent metallicity cutoff), whereas $p \rightarrow \infty$ characterizes no metallicity bias.

Figure 6 shows the evolution of the median UV luminosity in unit redshift bins of our sample in comparison to these models. The luminosity depth of our observations is a function of redshift (Figure 4), and we hence recalculated the median values given in Trenti et al. (2014) for the observed luminosity limits in each redshift bin. The faint limit was set to $M - 3\sigma(M)$ in each magnitude bin; specifically we compute the median UV luminosity between $-22.5 \leqslant M \leqslant -13.2$ at $z < 1$, $-22.5 \leqslant M \leqslant -16.7$ at $1 \leqslant z < 3$, $-22.5 \leqslant M \leqslant -17.2$ at $3 \leqslant z < 4.5$. Observed medians and their errors were estimated via a bootstrap method (30,000 samples), where each detected host was represented as a Gaussian centered on the measured

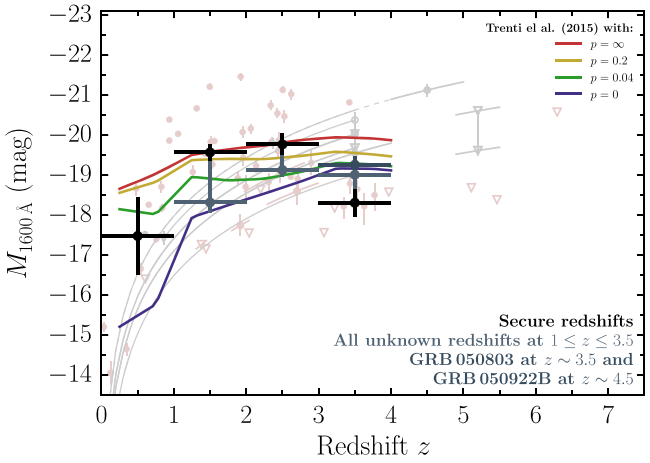

Figure 6. Evolution of the median obscured UV luminosity (in bins of unit redshift) with known redshift (black markers). Their errors were assessed through bootstrapping. At $z = 3$–4 the sample is characterized by a significant number of non-detections. Overlaid are model tracks for different strengths of a possible metallicity bias (Trenti et al. 2014). The hosts with unknown redshift were also put at $1 < z < 2$ and $2 < z < 3$ to assess their impact on the median value (displayed by lighter blue bars). The blue bar shows the median UV luminosity if GRBs 050803 and 050922B are put at $z = 3.5$ and $z = 4.5$, respectively (Section 3.3). See Section 4.2 for details.

luminosity with a width given by the measurement uncertainty. Non-detected hosts were drawn from a uniform distribution between a fiducial magnitude cut and the 3σ limiting detection.

Though we have only four data points with significant uncertainty, the data appear to favor models of GRB production incorporating significant levels of bias toward low metallicity hosts (as suggested by Vergani et al. 2014; Cucchiara et al. 2015). In particular, the inclusion of any of the hosts of unknown redshift in individual redshift bins always lowers the median magnitude in that bin. Note that these models of metallicity bias for GRB production, which include metallicity-dependent (single star collapsars) and independent channels (binary progenitor)[19] do not imply a fixed fraction of GRB production via each channel, but rather an evolving fraction with redshift, with the metallicity-dependent (collapsar type) channel always being dominant at high redshift (see Trenti et al. 2014 for full details).

4.3. The UV Luminosity Function

In order to go further than just analyzing the median properties of the TOUGH hosts, we construct LFs for GRB hosts from $z = 0$ to $z = 4.5$ in appropriate redshift and luminosity bins to compare both with those from LBG surveys and those predicted by the models of Trenti et al. (2014). We select those hosts from our sample that fall in the redshift ranges of the three LBGs surveys in Table 5, and in the range $0 < z < 1$.

Figure 7 shows which part of the $M_{1600\,\mathrm{\AA}}$–z parameter space is probed by LBG surveys. The evolution of $M_\star$ implies that GRB hosts probe the full luminosity range of LBGs between $z = 1$ and 3, whereas at lower and higher redshifts, GRBs rather probe the faint-end of the observed LBG LF. We note that the luminosity range of GRB host galaxies extends to much fainter galaxies between $z = 1$ and $z = 3$ than probed by the LBG surveys in Table 5. However, recent observations by Alavi et al. (2014) found no evidence for a change in the LBG LF parameters at $z \sim 2$ down to $M_{1500} = -15$ mag, which reassures us in extrapolating the LFs in Table 5 to lower luminosities.

Figure 8 displays the GRB host galaxy cumulative distributions for the four redshift intervals. Since GRBs are produced by the collapse of very massive stars, it has been suggested that GRBs should select galaxies according to their SFR. In the simplest model, Fynbo et al. (2002) proposed that the UV GRB-host LF should be similar to that of LBG samples weighted by their SFR, where the SFR is proportional to the *unobscured* UV luminosity, which can be expressed as SFR $\propto 10^{0.4 \times A_V(M_{\mathrm{obs}})}\, L_{\mathrm{obs}}$. Following Trenti et al. (2014), we use $A_V = 4.43 + 0.79\ \log(10)\ \sigma^2_{\beta_{\mathrm{UV}}} + 1.99\ \beta_{\mathrm{UV}}$ where $\sigma_{\beta_{\mathrm{UV}}} = 0.34$. The cumulative distributions of the SFR-weighted LBG LFs from Table 5 are overlaid in the same plot.

At low and high redshift, the observed distribution differs significantly from the no metallicity bias (or equivalently, LBG derived) model LFs. In the $3 < z < 4.5$ region, for example, we can reject the null hypothesis of the data being drawn from the SFR weighted LBG LF at a level of 0.01% via a Kolmogorov–Smirnov (KS) test. In the medium redshift ranges

Table 5
Parameters of LBG Luminosity Functions

Redshift Interval	Luminosity Interval (mag)	$M_{1600\,\mathrm{\AA},\star}$ (mag)	Faint-end Slope α	References
$1.0 \leqslant z \leqslant 1.5$	−21.50 to −17.83	−20.08 ± 0.36	−1.84 ± 0.15	(1)
$1.9 \leqslant z \leqslant 2.7$	−22.83 to −17.83	−20.70 ± 0.11	−1.73 ± 0.07	(2)
$3.0 \leqslant z \leqslant 4.5$	−22.69 to −15.94	−21.07 ± 0.08	−1.64 ± 0.04	(3)

Note. Values of LBG LFs in the Schechter parameterization for different redshift intervals. The redshift column shows the interval for which the LFs were applied to.
References. (1) Oesch et al. (2010), (2) Reddy & Steidel (2009) (3) Bouwens et al. (2014).

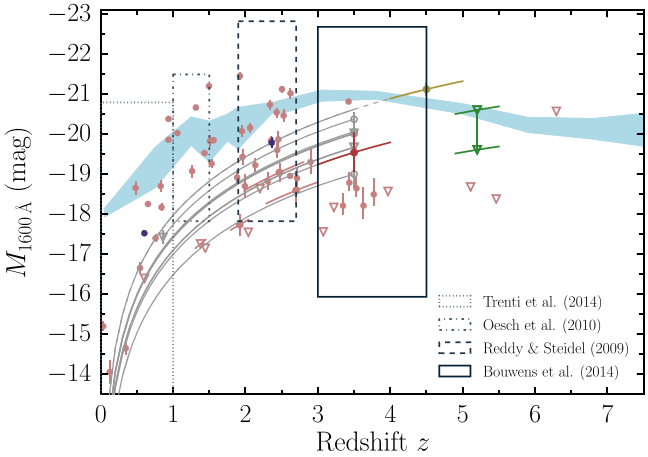

Figure 7. Observed luminosity evolution of GRB host galaxies and the evolution of $M_{1600\,\mathrm{\AA},\star}$ of LBGs (light-blue shaded area; Arnouts et al. 2005; Reddy & Steidel 2009; Oesch et al. 2010; Bouwens et al. 2014). Overlaid are the redshift and luminosity ranges probed by the LBG surveys in Table 5 at $z > 1$ and the predicted LBG LF for $z < 1$ by Trenti et al. (2014), which are used to construct the UV GRB-host luminosity function. The color coding is identical to Figure 4.

[19] Cantiello et al. (2007) argue that the binary channel may prefer low-metallicity environments as well, i.e., being metal dependent.

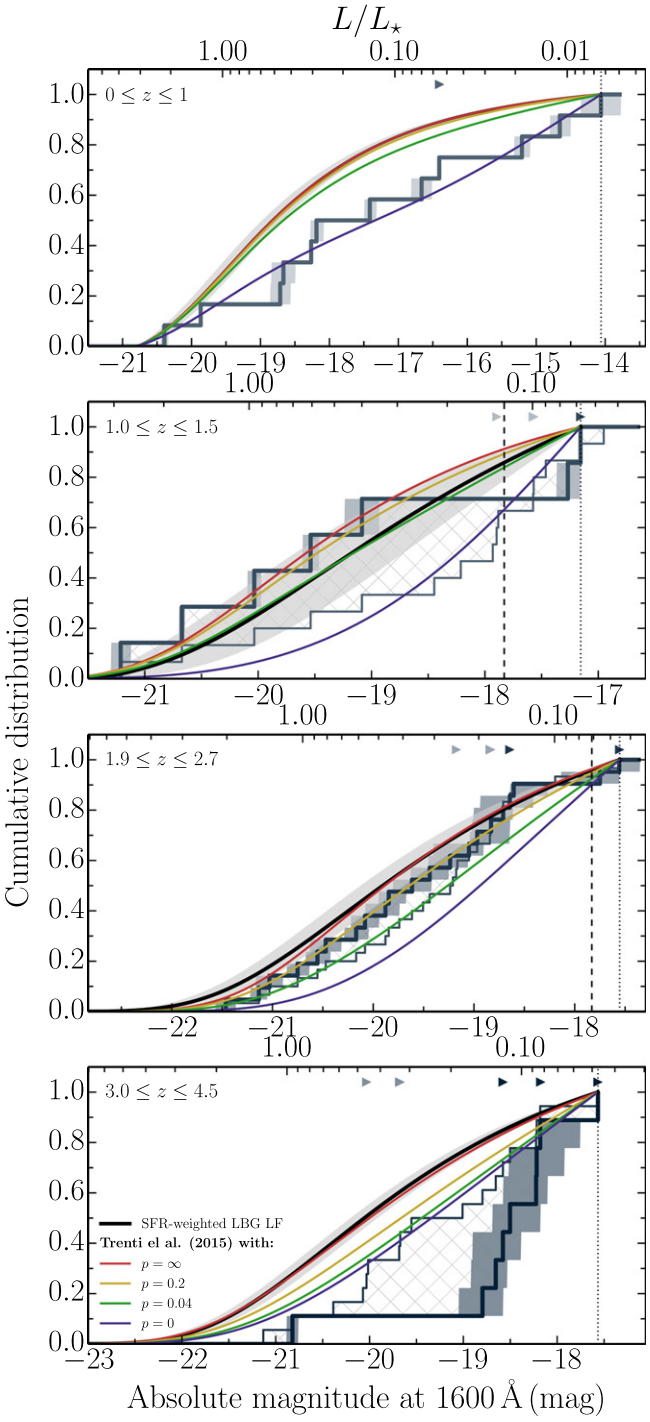

Figure 8. Observed cumulative distribution (CDF) of the TOUGH sample at different redshifts. The shaded areas display the 1σ uncertainties in the UV luminosity of the GRB host galaxies. The hatched regions show the parameter space between the two extreme cases of including/not including all hosts of unknown redshift in the respective redshift interval. The black curves display the CDFs of an SFR-weighted LBG luminosity function for the given redshift interval and their 1σ envelopes in gray. In color are shown the luminosity functions for various levels of metallicity bias predicted by Trenti et al. (2014). The limiting magnitudes of the LBG surveys are displayed by the dashed vertical lines and the dotted vertical lines indicate the magnitude of the faintest observed host in each sample, where the CDFs are formally normalized in each respective panel. The parameters of the LBG luminosity functions are listed in Table 5.

($1 < z < 1.5$ and $1.9 < z < 2.7$) the data are insufficient to distinguish reliably between any of the models, particularly due to some non-detections and the possibility of some of the hosts of unknown redshift being within these bins as discussed in the next section.

5. DISCUSSION

5.1. The Impact of Hosts with Unknown Redshifts

There are nine hosts in our sample with redshifts unknown within certain limits. As discussed in Jakobsson et al. (2012), a conservative upper limit of $z < 3.5$ can be placed on four of the bursts associated with these hosts via their measured excess (above Galactic) X-ray absorption following the method of Grupe et al. (2007). The remaining five bursts can be at higher redshifts (see Table 2 for details).

In this paper we set a formal redshift limit of $z < 3.5$ to avoid corrections for IGM and Lyα absorption. These unknown redshift hosts can therefore exist anywhere along the gray tracks plotted in the right-hand panel of Figure 4. The maximum plausible redshift of $z = 3.5$ is approximately coincident with the midpoint of our highest redshift LBG comparison sample, and in Figure 8 we also show the effect of placing all the unknown hosts at the midpoint of each LBG comparison range in turn (hatched regions). As can be seen from the bottom panel in this plot, if all unknown redshift hosts are actually at their highest plausible redshift, which may be a likely scenario (see Figure 11 in Hjorth et al. 2012), and all upper limits are treated as detections, then the likelihood (KS probability) of the TOUGH cumulative distribution being consistent with the SFR weighted LBG model rises to 1.0%. Note that this value represents our most conservative limit compared to the more flexible simulation discussed below.

To quantify how many of the TOUGH hosts with unknown redshift would be required to be within the range $3 \leqslant z \leqslant 3.5$ in order to make the TOUGH host LF consistent with the SFR-weighted LBG LF, we performed a Monte-Carlo simulation as follows. One of the nine hosts with unknown redshift was chosen at random and assigned a random redshift between $3 \leqslant z \leqslant 3.5$. The appropriate host luminosity was then drawn from a normal distribution centered around the observation value with a width (1σ) of the detection error for detected hosts, and a uniform distribution between the upper limit and the luminosity of the faintest host in the TOUGH $3 \leqslant z \leqslant 4.5$ sample for those hosts with an upper limit only. This host is added to the TOUGH CDF, and a KS value computed between the new CDF and the SFR weighted LBG-LF. The process is repeated 30,000 times and a mean and median KS value obtained. We then successively add hosts of unknown redshift and repeat the procedure until all nine hosts are included in the CDF. Figure 9 shows how the measured KS value varies with the number of added hosts of unknown redshift.

As can be seen from Figure 9, at least 3 unknown hosts are required for the TOUGH distribution to fall below the 3σ equivalent rejection probability level of <0.3% chance of consistency with being drawn from the SFR-weighted LBG (no metallicity bias) LF model. Even when all unknown redshift hosts are included in the simulation, the median KS probability of the distributions being consistent is only 0.8%. The gap may be closed further if some of the unknown hosts are at higher redshifts still ($3.5 < z < 4.5$) since their *R*-band observations then would have been significantly affected by IGM and Lyα absorption. Nevertheless, the metallicity dependent models of

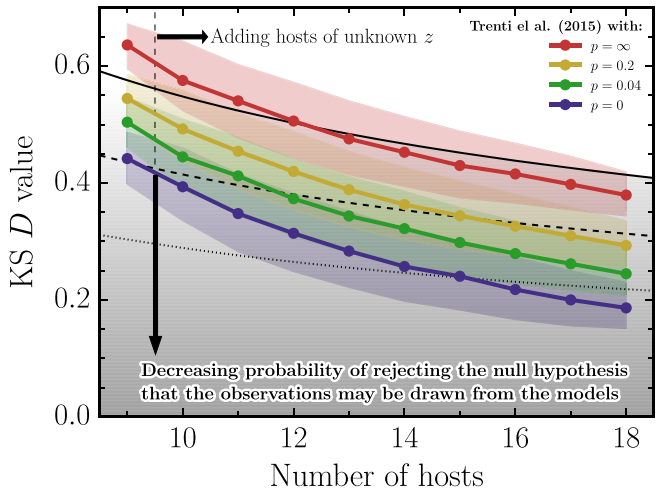

Figure 9. Kolmogorov–Smirnov test between the observed TOUGH hosts and the various luminosity functions between $z = 3.0$ and $z = 4.5$ as the number of hosts with unknown redshift is increased. The color-shaded regions represent the 16 and 84 percentiles of the MC simulations. With the null hypothesis that the data may be drawn from the respective model LF, the white area of the plot represents rejection of this null hypothesis with a probability level of it being correct of <0.3% (3σ equivalent). Within the gray shaded region, the dashed and dotted lines display the 5% (2σ equivalent) and 32% (1σ equivalent) rejection levels respectively. See Section 5.1 for details.

Trenti et al. (2014) appear a better fit to the data, with critical KS rejection levels much lower.

We emphasize again that these models do not represent a fixed fraction of GRB production via metal-dependent and independent channels, but are derived from stellar population syntheses combined with a GRB production efficiency model with respect to metallicity controlled by the value of p. Lower (but non-zero) p values represent a stronger level of bias toward low metallicity hosts, as expected from the collapsar model. We note that the $p = 0$ model (blue lines) which represents a stringent metallicity plateau for GRB production is effectively ruled out by observations of some high metallicity GRB hosts (e.g., Levesque et al. 2010; Elliott et al. 2013; Schulze et al. 2014), and are plotted as convenient limits for comparison only.

5.2. Influence of Selection Effects on Previous GRB Host Samples

The TOUGH sample is independent of the brightness of the optical afterglow, but the properties of the prompt emission could still bias the sample toward a certain GRB population and hence a certain host galaxy population. We find no correlation between the host properties and energy released at γ-ray energies, $E_{\rm iso}$ (values taken from Butler et al. 2007), or the peak flux photon flux (taken from Sakamoto et al. 2008) at any redshift. At low redshift (where we are sampling the greatest proportion of the GRB γ-ray LF itself) there is also no tendency for brighter bursts to favor dimmer hosts, and we therefore do not believe any flux-limited observational bias of the bursts themselves significantly affects any of our conclusions regarding the hosts.

Previous GRB host surveys have tended to be biased toward bursts with optically brighter afterglows and/or hosts, whereas the TOUGH sample (as stressed throughout this work) is independent of the optical properties of bursts or hosts. To examine whether these previous observational biases are significant or not, we investigate whether the same conclusions could be drawn from a previous heterogeneous sample. To address this question we retrieved all host measurements that probe the rest-frame UV continuum from the GHostS database (Savaglio 2006). Until 2012 January (before the first results from the TOUGH survey were published), the database comprised observations for over 120 hosts. As an example, we build the UV luminosity distributions for this sample and divide them into the same redshift and luminosity bins as the TOUGH sample.

The observed cumulative distributions are shown in the lower panels of Figure 10, along with those of the TOUGH sample in the upper panels. At all redshifts, except perhaps for $1 < z < 1.5$, we see an overabundance of luminous galaxies in the GHostS sample compared to TOUGH. This clearly shows that selection effects from GRB afterglow observations must be carefully taken into account before attempting to extract any ensemble properties. The limiting magnitudes in the GHostS sample are in general also significantly shallower than ours. To be able to extract any meaningful results, GRB-selected galaxy samples need to be carried out to the magnitude limits of LBG surveys, i.e., reaching at least $R \sim 28$ mag.

5.3. Origin of the Redshift Evolution of the Luminosity Function

Our findings let us draw the following picture. GRBs probe the full luminosity range (and below) of LBG surveys at all comparable redshifts. Furthermore, throughout the entire redshift range of our sample, GRB hosts appear consistent with models of GRBs being produced by a combination of a metal-dependent (single star collapsar) channel and an independent (binary progenitor) channel with a relatively high level of bias (low, but non-zero value of p) toward low metallicity hosts (Trenti et al. 2014), though we cannot completely rule out the unbiased models in the range $1 < z < 3$. This behavior may also lend support to the model of the starvation of infalling pristine gas at $z \sim 1$–1.5 proposed by Perley et al. (2013), moving the GRB host population away from LBG galaxies as a whole to low-mass UV faint galaxies as redshift decreases.

At $z > 3$, we observe a lack of UV luminous GRB hosts. All detected hosts (except one) are at least 3 mag fainter than $L_\star$ galaxies. If GRB hosts were truly similar to LBGs, we may expect this connection to improve at higher redshifts, where any potential metallicity bias becomes less important in comparison to the overall galaxy population. Indeed the presence of a reasonable fraction of the nine hosts of unknown redshift in this range would reduce this lack of bright hosts, though not entirely to the level of consistency with an SFR weighted LBG LF.

Thus it would seem that at both high and low redshift, TOUGH supports the idea that GRBs are preferentially found in low-metallicity, relatively UV faint hosts compared to the overall galaxy population, and therefore their relationship to the cosmic SFR density history as measured by UV flux limited surveys is not simple. Several previous studies have pointed to the numbers of GRBs observed at high redshift indicating a large amount of hidden (massive) star formation in galaxies that are too faint to be detected in current LBG surveys (Fynbo et al. 1999; Haehnelt et al. 2000; Fynbo et al. 2002; Le Floc'h et al. 2003; Jakobsson et al. 2005, 2012; Kistler et al. 2008; Schmidt 2009).

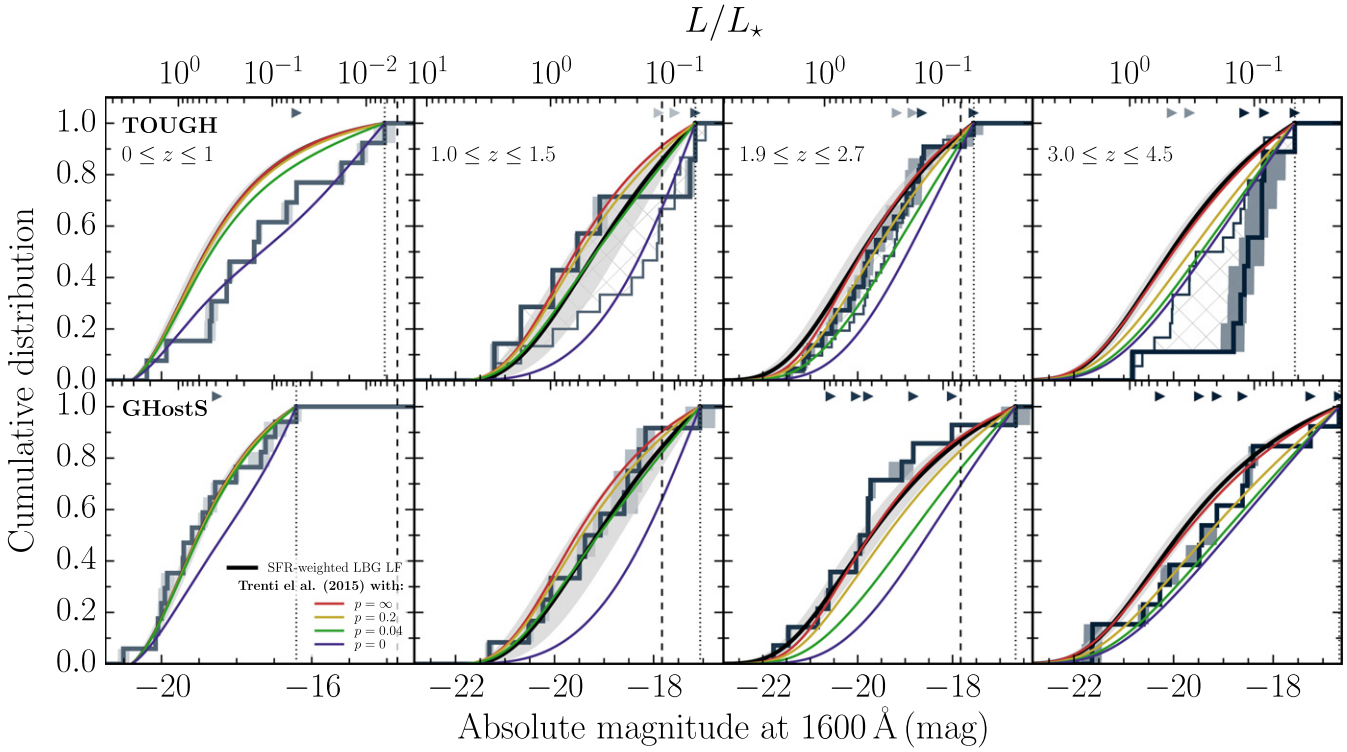

Figure 10. Observed CDFs of the heterogeneous GHostS (bottom) sample in comparison to the optically unbiased TOUGH (top) sample at different redshifts. There are clear differences between the two host samples, particularly at high z (see text for discussion). The hatched regions show the parameter space between the two extreme cases of including/not including all hosts of unknown redshift in the respective redshift interval. The black curves display the CDFs of an SFR-weighted LBG luminosity function for the given redshift interval and their 1σ envelopes in gray. In color are shown the luminosity functions for various levels of metallicity bias predicted by Trenti et al. (2014). The plot boundaries were adjusted to the luminosity range of the respective LBG survey and Trenti et al. (2014). The thick line shown in light blue in the $3 \leqslant z \leqslant 4.5$ panel indicates the luminosity function, if all hosts with unknown redshift would be at $z = 3.5$, and GRBs 050805 and 050922B at $z = 3.5$ and $z = 4.5$, respectively. The limiting magnitudes of the LBG surveys are displayed by the dashed vertical lines and the dotted vertical lines indicate the magnitude of the faintest observed host in each sample, where the CDFs are formally normalized in each respective panel. The parameters of the LBG luminosity functions are listed in Table 5.

Alternatively others have suggested that GRB production efficiency with respect to star formation may increase with redshift (Kistler et al. 2009; Butler et al. 2010; Robertson & Ellis 2012; Salvaterra et al. 2012). If this latter alternative of increased GRB efficiency were the sole reason for the change, however, one might expect to still see some bright hosts at high redshift. However, highly star-forming galaxies may well also contain a large amount of dust, both obscuring their intrinsic SFR and making it more difficult to obtain spectroscopic redshifts. Despite targeted and deep searches, no GRB host has yet been detected beyond $z \sim 5$, which lends support to the lack of bright hosts at high redshift not being an artifact of our survey. Obviously since high-z GRBs are rare, the influence of small number statistics cannot be avoided. We suggest however, that though an increase in GRB production efficiency with respect to the UV measured cosmic SFR density at high redshift may be a useful calculational tool in simulation studies, it does not represent the detailed picture regarding individual GRB host galaxies, and more unbiased GRB host data are required.

During the review process of this paper, other workers have submitted investigations of the properties of GRB host galaxies. Greiner et al. (2015) presented discussions of the properties of a *heterogeneous* sample of GRB hosts at $z \sim 3$, and Perley et al. (2015b) presented findings on the NIR luminosity distribution $z = 0$ to $z = 5$ from the optically unbiased *Swift* Gamma-Ray Burst Host Galaxy Legacy Survey (SHOALS; Perley et al. 2015a). While the former study concludes that GRBs are unbiased tracers of star formation (compare our Section 5.2 and Figure 10), the latter study comes to a similar conclusion to that presented in this paper: GRB hosts in general appear fainter than a model that solely depends on SFR would predict, with a particularly pronounced lack of NIR luminous galaxies at $z < 1$. In all three samples, the number of events at $z > 4$ is relatively small, illustrating the need for a more concerted observational effort targeting this regime.

6. CONCLUSION

We have used the optically unbiased TOUGH sample to examine the UV GRB host galaxy LF from $z = 0$ to $z = 6.3$. We find the TOUGH host LF to be most compatible at all redshifts with an SFR weighted LF derived from a model containing both a metal-independent (binary progenitor) and metal-dependent (single star collapsar) channels with a relatively high level of bias toward low-metallicity hosts as suggested in Kocevski & West (2011), Graham & Fruchter (2013), Perley et al. (2013), Trenti et al. (2014), Vergani et al. (2014), and Cucchiara et al. (2015). This is particularly the case at low $(0 < z < 1)$ and high $(3 < z < 4.5)$ redshifts, though we cannot rule out an unbiased LF at medium redshifts $(1 < z < 3)$ as observed in more heterogeneous samples with unknown observational biases.

At high redshifts $(3 < z < 4)$ in particular, the lack of detected UV luminous host galaxies combined with the

likelihood that several (if not all) of the nine hosts of unknown redshifts may be in this range show that a deep spectroscopic survey with an optical+NIR spectrograph such as the ESO X-shooter UV–NIR echellete spectrograph is needed to fully constrain the GRB host LF and elucidate more fully the relationship between GRBs and the cosmic SFR density history.

We thank the referee for a careful reading of the manuscript and for helpful comments that improved this paper. We acknowledge with sadness the recent unexpected passing of our colleague and co-author Javier Gorosabel. His support of and contributions to this work and astronomy in general are greatly appreciated. We thank Stephanie Courty and Daniele Malesani for fruitful discussions. We also thank Daniele Malesani for kindly providing the TNG data and Michele Trenti for providing the parameterization of the spectral slope. S. Schulze acknowledges support from CONICYT-Chile FONDECYT 3140534, Basal-CATA PFB-06/2007, and Project IC120009 "Millennium Institute of Astrophysics (MAS) of Iniciativa Científica Milenio del Ministerio de Economía, Fomento y Turismo, by a Grant of Excellence from the Icelandic Research Fund, and from the University of Iceland Research Fund. R.C. is grateful to the University of Hertfordshire for travel support. The research activity of AdUP and J.G. is supported by Spanish research project AYA2012-39362-C02-02. AdUP acknowledges support by the European Commission under the Marie Curie Career Integration Grant program (FP7-PEOPLE-2012-CIG 322307). The Dark Cosmology Centre is funded by the Danish National Research Foundation. The research leading to these results has received funding from the European Research Council under the European Union's Seventh Framework Program (FP7/2007-2013)/ERC Grant agreement no. EGGS-278202. This research has made use of the GHostS database (www.grbhosts.org), which is partly funded by *Spitzer*/NASA grant RSA Agreement No. 1287913. Based in part on observations collected with the NASA/ESA *Hubble Space Telescope*, obtained at the Space Telescope Science Institute, which is operated by the Association of Universities for Research in Astronomy, Inc., under NASA contract NAS 5-26555, as part of the programs 11734, 12307, 11734, with the Gemini Observatory, which is operated by the Association of Universities for Research in Astronomy, Inc., under a cooperative agreement with the NSF on behalf of the Gemini partnership, as part of the programs GS-2007B-Q-1, GS-2013B-Q-69, and GS-2014A-Q-6, the Gran Telescopio Canarias (GTC), installed in the Spanish Observatorio del Roque de los Muchachos of the Instituto de Astrofísica de Canarias, in the island of La Palma, with the Italian Telescopio Nazionale Galileo (TNG) operated on the island of La Palma by the Fundación Galileo Galilei of the INAF (Istituto Nazionale di Astrofisica) at the Spanish Observatorio del Roque de los Muchachos of the Instituto de Astrofisica de Canarias as part of the programs A22TAC-107, with the 2.2-m MPG telescope on La Silla as part of the program CN2014B-102, and with the *Spitzer Space Telescope*, which is operated by the Jet Propulsion Laboratory, California Institute of Technology under a contract with NASA, as part of the program 57753, Some of the data presented herein were obtained at the W.M. Keck Observatory, which is operated as a scientific partnership among the California Institute of Technology, the University of California, and the National Aeronautics and Space Administration. The observatory was made possible by the generous financial support of the W.M. Keck Foundation. Part of the funding for GROND was generously granted from the Leibniz-Prize to Prof. G. Hasinger (DFG grant HA 1850/28-1). Funding for SDSS-III has been provided by the Alfred P. Sloan Foundation, the Participating Institutions, the National Science Foundation, and the U.S. Department of Energy Office of Science. The SDSS-III web site is http://www.sdss3.org/. SDSS-III is managed by the Astrophysical Research Consortium for the Participating Institutions of the SDSS-III Collaboration including the University of Arizona, the Brazilian Participation Group, Brookhaven National Laboratory, Carnegie Mellon University, University of Florida, the French Participation Group, the German Participation Group, Harvard University, the Instituto de Astrofisica de Canarias, the Michigan State/Notre Dame/JINA Participation Group, Johns Hopkins University, Lawrence Berkeley National Laboratory, Max Planck Institute for Astrophysics, Max Planck Institute for Extraterrestrial Physics, New Mexico State University, New York University, Ohio State University, Pennsylvania State University, University of Portsmouth, Princeton University, the Spanish Participation Group, University of Tokyo, University of Utah, Vanderbilt University, University of Virginia, University of Washington, and Yale University.

REFERENCES

Afonso, P., Greiner, J., Pian, E., et al. 2011, A&A, 526, A154
Aihara, H., Allende Prieto, C., An, D., et al. 2011, ApJS, 193, 29
Alavi, A., Siana, B., Richard, J., et al. 2014, ApJ, 780, 143
Arnouts, S., Cristiani, S., Moscardini, L., et al. 1999, MNRAS, 310, 540
Arnouts, S., Schiminovich, D., Ilbert, O., et al. 2005, ApJL, 619, L43
Bertin, E., & Arnouts, S. 1996, A&AS, 117, 393
Blanton, M. R., & Roweis, S. 2007, AJ, 133, 734
Bloom, J. S., Kulkarni, S. R., & Djorgovski, S. G. 2002, AJ, 123, 1111
Bouwens, R. J., Illingworth, G. D., Franx, M., & Ford, H. 2007, ApJ, 670, 928
Bouwens, R. J., Illingworth, G. D., Franx, M., et al. 2009, ApJ, 705, 936
Bouwens, R. J., Illingworth, G. D., Oesch, P. A., et al. 2010a, ApJL, 709, L133
Bouwens, R. J., Illingworth, G. D., Oesch, P. A., et al. 2010b, ApJL, 708, L69
Bouwens, R. J., Illingworth, G. D., Oesch, P. A., et al. 2012, ApJ, 754, 83
Bouwens, R. J., Illingworth, G. D., Oesch, P. A., et al. 2014, ApJ, 793, 115
Breeveld, A. A., Landsman, W., Holland, S. T., et al. 2011, in AIP Conf. Ser. 1358, ed. J. E. McEnery, J. L. Racusin & N. Gehrels (Melville, NY: AIP), 373
Bruzual, G., & Charlot, S. 2003, MNRAS, 344, 1000
Butler, N. R., Bloom, J. S., & Poznanski, D. 2010, ApJ, 711, 495
Butler, N. R., Kocevski, D., Bloom, J. S., & Curtis, J. L. 2007, ApJ, 671, 656
Calzetti, D., Armus, L., Bohlin, R. C., et al. 2000, ApJ, 533, 682
Cantiello, M., Yoon, S.-C., Langer, N., & Livio, M. 2007, A&A, 465, L29
Carilli, C. L., & Walter, F. 2013, ARA&A, 51, 105
Chen, H.-W., Perley, D. A., Pollack, L. K., et al. 2009, ApJ, 691, 152
Chen, H.-W. 2012, MNRAS, 419, 3039
Christensen, L., Hjorth, J., & Gorosabel, J. 2004, A&A, 425, 913
Cucchiara, A., Fumagalli, M., Rafelski, M., et al. 2015, ApJ, 804, 51
Daddi, E., Dickinson, M., Morrison, G., et al. 2007, ApJ, 670, 156
Elbaz, D., Dickinson, M., Hwang, H. S., et al. 2011, A&A, 533, A119
Elliott, J., Greiner, J., Khochfar, S., et al. 2012, A&A, 539, A113
Elliott, J., Krühler, T., Greiner, J., et al. 2013, A&A, 556, A23
Erb, D. K., Shapley, A. E., Pettini, M., et al. 2006, ApJ, 644, 813
Finkelstein, S. L., Papovich, C., Salmon, B., et al. 2012, ApJ, 756, 164
Foster, C., Hopkins, A. M., Gunawardhana, M., et al. 2012, A&A, 547, A79
Fruchter, A. S., Levan, A. J., Strolger, L., et al. 2006, Natur, 441, 463
Fynbo, J. P. U., Jakobsson, P., Prochaska, J. X., et al. 2009, ApJS, 185, 526
Fynbo, J. P. U., Möller, P., Thomsen, B., et al. 2002, A&A, 388, 425
Fynbo, J. U., Møller, P., & Warren, S. J. 1999, MNRAS, 305, 849
Graham, J. F., & Fruchter, A. S. 2013, ApJ, 774, 119
Greiner, J., Bornemann, W., Clemens, C., et al. 2008, PASP, 120, 405
Greiner, J., Fox, D. B., Schady, P., et al. 2015, ApJ, submitted (arXiv:1503.05323)
Grupe, D., Nousek, J. A., vanden Berk, D. E., et al. 2007, AJ, 133, 2216
Haehnelt, M. G., Steinmetz, M., & Rauch, M. 2000, ApJ, 534, 594

Hathi, N. P., Cohen, S. H., Ryan, R. E., Jr., et al. 2013, ApJ, 765, 88
Hathi, N. P., Malhotra, S., & Rhoads, J. E. 2008, ApJ, 673, 686
Hjorth, J., Malesani, D., Jakobsson, P., et al. 2012, ApJ, 756, 187
Hogg, D. W., Pahre, M. A., McCarthy, J. K., et al. 1997, MNRAS, 288, 404
Hopkins, A. M. 2004, ApJ, 615, 209
Hopkins, A. M., & Beacom, J. F. 2006, ApJ, 651, 142
Hunt, L. K., Palazzi, E., Michałowski, M. J., et al. 2014, A&A, 565, A112
Ilbert, O., Arnouts, S., McCracken, H. J., et al. 2006, A&A, 457, 841
Jakobsson, P., Björnsson, G., Fynbo, J. P. U., et al. 2005, MNRAS, 362, 245
Jakobsson, P., Hjorth, J., Malesani, D., et al. 2012, ApJ, 752, 62
Kistler, M. D., Yüksel, H., Beacom, J. F., Hopkins, A. M., & Wyithe, J. S. B. 2009, ApJL, 705, L104
Kistler, M. D., Yüksel, H., Beacom, J. F., & Stanek, K. Z. 2008, ApJL, 673, L119
Kocevski, D., & West, A. A. 2011, ApJL, 735, L8
Koekemoer, A. M., Fruchter, A. S., Hook, R. N., & Hack, W. 2003, in *HST* Calibration Workshop, Hubble after the Installation of the ACS and the NICMOS Cooling System, ed. S. Arribas, A. Koekemoer & B. Whitmore, 337
Kohn, S. A., Michałowski, M. J., Bourne, N., et al. 2015, MNRAS, 448, 1494
Krühler, T., Greiner, J., Schady, P., et al. 2011, A&A, 534, A108
Krühler, T., Küpcü Yoldaş, A., Greiner, J., et al. 2008, ApJ, 685, 376
Krühler, T., Greiner, J., Schady, P., et al. 2012, ApJ, 758, 46
Krühler, T., Malesani, D., Fynbo, J. P. U., et al. 2015, A&A, in press (arXiv:1505.06743)
Larson, D., Dunkley, J., Hinshaw, G., et al. 2011, ApJS, 192, 16
LeFloc'h, E., Duc, P. A., Mirabel, I. F., et al. 2003, A&A, 400, 499
Lee, H., Skillman, E. D., Cannon, J. M., et al. 2006, ApJ, 647, 970
Levesque, E. M., Kewley, L. J., Graham, J. F., & Fruchter, A. S. 2010, ApJL, 712, L26
Magdis, G. E., Rigopoulou, D., Huang, J.-S., & Fazio, G. G. 2010, MNRAS, 401, 1521
Mangano, V., Holland, S. T., Malesani, D., et al. 2007, A&A, 470, 105
Meurer, G. R., Heckman, T. M., & Calzetti, D. 1999, ApJ, 521, 64
Michałowski, M. J., Hjorth, J., Castro Cerón, J. M., & Watson, D. 2008, ApJ, 672, 817
Michałowski, M. J., Kamble, A., Hjorth, J., et al. 2012, ApJ, 755, 85
Milvang-Jensen, B., Fynbo, J. P. U., Malesani, D., et al. 2012, ApJ, 756, 25
Modjaz, M., Kewley, L., Kirshner, R. P., et al. 2008, AJ, 135, 1136
Noeske, K. G., Weiner, B. J., Faber, S. M., et al. 2007, ApJL, 660, L43
Oesch, P. A., Bouwens, R. J., Carollo, C. M., et al. 2010, ApJL, 725, L150
Perley, D. A., Cenko, S. B., Bloom, J. S., et al. 2009, AJ, 138, 1690
Perley, D. A., Krühler, T., Schulze, S., et al. 2015b, ApJ, submitted (arXiv:1504.02482)
Perley, D. A., Levan, A. J., Tanvir, N. R., et al. 2013, ApJ, 778, 128
Perley, D. A., Tanvir, N. R., Hjorth, J., et al. 2015a, ApJ, submitted (arXiv:1504.02479)
Pettini, M., Rix, S. A., Steidel, C. C., et al. 2002, ApJ, 569, 742
Pettini, M., Shapley, A. E., Steidel, C. C., et al. 2001, ApJ, 554, 981
Reddy, N. A., & Steidel, C. C. 2009, ApJ, 692, 778
Robertson, B. E., & Ellis, R. S. 2012, ApJ, 744, 95
Rodighiero, G., et al. 2010, A&A, 518, L25
Rossi, A., Klose, S., Ferrero, P., et al. 2012, A&A, 545, A77
Sakamoto, T., Barthelmy, S. D., Barbier, L., et al. 2008, ApJS, 175, 179
Salvaterra, R., della Valle, M., Campana, S., et al. 2009, Natur, 461, 1258
Salvaterra, R., Campana, S., Vergani, S. D., et al. 2012, ApJ, 749, 68
Savaglio, S. 2006, NJPh, 8, 195
Savaglio, S., Glazebrook, K., le Borgne, D., et al. 2005, ApJ, 635, 260
Savaglio, S., Glazebrook, K., & Le Borgne, D. 2009, ApJ, 691, 182
Schady, P., Savaglio, S., Müller, T., et al. 2014, A&A, 570, A52
Schaerer, D., de Barros, S., & Sklias, P. 2013, A&A, 549, A4
Schiminovich, D., Ilbert, O., Arnouts, S., et al. 2005, ApJL, 619, L47
Schlegel, D. J., Finkbeiner, D. P., & Davis, M. 1998, ApJ, 500, 525
Schmidt, M. 2009, ApJ, 700, 633
Schulze, S., Fynbo, J. P. U., Milvang-Jensen, B., et al. 2012, A&A, 546, A20
Schulze, S., Malesani, D., Cucchiara, A., et al. 2014, A&A, 566, A102
Scoville, N., Aussel, H., Brusa, M., et al. 2007, ApJS, 172, 1
Shapley, A. E. 2011, ARA&A, 49, 525
Sirianni, M., Jee, M. J., Benítez, N., et al. 2005, PASP, 117, 1049
Stanek, K. Z., Gnedin, O. Y., Beacom, J. F., et al. 2006, AcA, 56, 333
Steidel, C. C., Giavalisco, M., Pettini, M., Dickinson, M., & Adelberger, K. L. 1996, ApJL, 462, L17
Tanvir, N. R., Barnard, V. E., Blain, A. W., et al. 2004, MNRAS, 352, 1073
Tanvir, N. R., Fox, D. B., Levan, A. J., et al. 2009, Natur, 461, 1254
Tanvir, N. R., Levan, A. J., Fruchter, A. S., et al. 2012, ApJ, 754, 46
Tody, D. 1986, Proc. SPIE, 627, 733
Tremonti, C. A., Heckman, T. M., Kauffmann, G., et al. 2004, ApJ, 613, 898
Trenti, M., Perna, R., & Jimenez, R. 2014, ApJ, submitted (arXiv:1406.1503)
Vergani, S. D., Salvaterra, R., Japelj, J., et al. 2014, A&A, submitted (arXiv:1409.7064)
Wolfe, A. M., Gawiser, E., & Prochaska, J. X. 2005, ARA&A, 43, 861
Woosley, S. E. 2011, arXiv:1105.4193
Yoldaş, A. K., Krühler, T., Greiner, J., et al. 2008, in AIP Conf. Ser. 1000, ed. M. Galassi, D. Palmer & E. Fenimore (Melville, NY: AIP), 227